Residual error correction for reducing the uncertainty of a sample-tracking robotic 3D measurement system

Daniel Wertjanz, Thomas Kern, Ernst Csencsics, and Georg Schitter

Advanced Mechatronic Systems Group, Automation and Control Institute (ACIN), TU Wien, 1040 Vienna (e-mail: {wertjanz,kern,csencsics,schitter}@acin.tuwien.ac.at)

Abstract: This paper presents a method for post-correction of disturbing relative motion between a robotic 3D measurement system and a sample under test. The active sample-tracking measurement platform carries a high-precision scanning confocal chromatic sensor acts as an end-effector of a robot, targeted for operation in a vibration-prone environment. The proposed method does not require any additional hardware and enables a point-by-point correction of the sequentially acquired 3D point cloud by the measured residual sample-tracking error. For experimental measurements at the maximum frame rate of 1 fps in a workshop-like environment, which induces a resonant 47 Hz relative motion, the axial measurement error and uncertainty is reduced by 20% to 0.19 µm and 0.25 µm, respectively.

Keywords: Mechatronic systems, robotic 3D measurement systems, scanning optical sensors, motion compensation and correction, application of mechatronic principles, design methodologies

1. INTRODUCTION

High-precision 3D measurements on the single- and sub-micrometer scale play an increasingly important role in quality control processes of the high-tech manufacturing industry [Imkamp et al. (2012)]. To enable a continuous and 100 % quality monitoring of industrially produced goods, flexible, fast and precise inline measurement systems are highly demanded [Schwenke et al. (2002)]. Besides increasing the overall throughput and the production yield, inline measurement systems can provide realtime optimization of production parameters to significantly enhance product reliability and quality [Gao et al. (2019); Grasso and Colosimo (2017)]. Especially, precise inline 3D measurements on freeform surfaces [Savio et al. (2007)] are a key technology for future production, ranging from the semiconductor to the automotive and consumer electronics sector [Yogeswaran and Payeur (2012); Yao et al. (2016)]. In particular, optically scanning 3D measurement systems, which dynamically acquire information about the sample on a point-by-point basis, have gained increasing attention due to their increased versatility [Schlarp et al. (2020)].

By employing industrial robots, flexible 3D measurements are enabled by aligning the measurement tool (MT) to arbitrary measurement locations on a sample surface [Rejc et al. (2009)]. However, robots themselves are lacking the required positioning precision for the demanded 3D surface measurements on the single- or even sub-micrometer scale [Csencsics et al. (2022)]. Currently, industrial robots achieve a precision of several tens of micrometers [Schneider et al. (2014)], which limits the achievable resolution of robotic 3D measurement systems to the same order of magnitude [de Sousa et al. (2017); Naverschnigg et al. (2022)]. Another challenge of integrating a precision 3D MT directly into an industrial production line are environmental vibrations, e.g. generated by running motors. Similar to the limited positioning precision of an industrial robot, these vibrations cause relative motion between the MT and the sample surface. As a result, 3D measurements are corrupted on the micrometer scale due to motion blur [Saathof et al. (2017)], making a 100% inline quality control of produced goods with structural sizes in the single-micrometer range infeasible feasible.

Recently, an active sample-tracking measurement system for precise robotic inline 3D sample inspection has been reported [Wertjanz et al. (2022)]. By means of feedback control, the integrated measurement platform (MP) maintains a constant alignment of the scanning confocal chromatic sensor (SCCS) [Wertjanz et al. (2021)] relative to the sample surface. The control-induced and contactless stiff link between SCCS and sample significantly reduces the disturbing relative motion and establishes local lab-like conditions, enabling robotic 3D measurements on the sub-micrometer scale. However, for high relative motion dynamics, a residual sample-tracking error remains, which is a limiting factor for the achievable measurement uncertainty.

⋆ This project is partially funded by the Hochschuljubilaeumsfonds of the city of Vienna, Austria under the project number H-260744/2020. The financial support by the Austrian Federal Ministry for Digital and Economic Affairs, and the National Foundation for Research, Technology and Development, as well as MICRO-EPSILON MESSTECHNIK GmbH & Co. KG and ATENSOR Engineering and Technology Systems GmbH is gratefully acknowledged.

Post-print version of the article: D. Wertjanz, T. Kern, E. Csencsics, and G. Schitter, "Residual error correction for reducing the uncertainty of a sample-tracking robotic 3D measurement system," *IFAC-PapersOnLine*, vol. 56 (2), 2023, pp. 4418-4423, 2023. DOI: 10.1016/j.ifacol.2023.10.1829

The contribution of this paper is the design and experimental validation of a residual tracking error correction method to reduce the uncertainty of a high-precision robotic 3D measurement system.

In order to increase the resolution of motion blur-corrupted measurements, motion correction algorithms can be employed in a post-processing manner [Fergus et al. (2006)]. For sequentially scanned optical sensors, such as the SCCS, a synchronized point-by-point correction of the measured relative motion between SCCS and sample appears as a valid approach [Schitter and Stemmer (2002)].

2. ROBOTIC 3D MEASUREMENT SYSTEM

In Fig. 1, the cross-sectional view of the high-precision robotic 3D measurement system's CAD model is shown. Acting as a robotic end-effector, the system design comprises an electromagnetically levitated and actuated MP, in which a SCCS [Wertjanz et al. (2021)] is integrated as high precision 3D MT. Using voice coil actuators (VCAs), quasi-zero stiffness actuation is achieved, which mechanically decouples the MP from the robot arm. The SCCS includes a fast steering mirror (FSM), which manipulates the optical path of a confocal chromatic sensor (CCS) to precisely scan the CCS' measuring light spot across the sample surface. For the FSM in center position, the optical path length of the measurement spot (MS) is equal to d_0.

High-precision tracking sensors (TSs) measure the relative position to the sample surface. By means of feedback control, this position is maintained constant, introducing a contactless stiff link between SCCS and sample, compensating vibration- as well as robot-induced disturbances (tracking control). In each degree of freedom (DoF), a tracking control bandwidth of 450 Hz is achieved. In this way, local lab-like conditions are established directly in the challenging environment of an industrial production line during a precision 3D measurement. With the additional internal position sensors (IPSs) measuring the relative position between MP and the robot arm, the MP can be stabilized in a free-floating position when the robot is repositioning and the TSs are out of range (stabilization mode).

Figure 2 presents the implemented system prototype. The high-precision 3D measurement module is mounted to an industrial 6-axis robot arm (KR 10 R900-2, KUKA AG, Augsburg, Germany). The IPS system comprises six capacitive displacement sensors (CSH05, Micro-Epsilon Messtechnik, Ortenburg, Germany), while the out-of-plane TS system uses three of the same type. Relative in-plane sample motion is measured by a position-sensitive device (PSD)-based sensing system, which uses laser diodes as markers [Wertjanz et al. (2022)]. Due to the different position sensing principles, the measured translational out-of-plane DoF position uncertainty of about 25 nm is one order of magnitude smaller than the uncertainty of the in-plane DoFs.

The SCCS [Wertjanz et al. (2021)] integrates a compact FSM with a high precision CCS (IFS2404, Micro-Epsilon Optronic, Dresden, Germany). A lateral scan area of about $350 \times 250\,\mu m^2$ can be imaged with frame rates of up to 1 fps, while providing a lateral and axial resolution of down to 2.5 µm and 76 nm for lower frame rates.

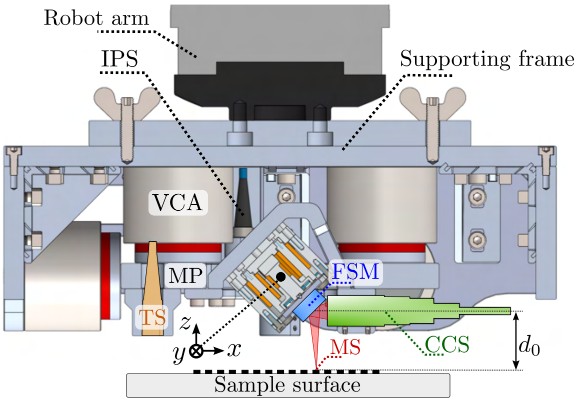

Fig. 1. Robotic 3D measurement module. The MP is actuated within the air gaps of the VCAs. TSs and IPSs measure the MP's position relative to the sample surface and supporting frame, respectively. An FSM manipulates the optical path of the CCS to scan the MS across the sample surface.

The data acquisition as well as the entire control architecture is implemented on a rapid prototyping system (MicroLabBox, dSPACE GmbH, Paderborn, Germany) with a sampling frequency of 25 kHz. In order to ensure a sufficiently low shutter time of the CCS, a measurement rate of 50 kHz is selected. The oversampling of the CCS further enables an averaging of two measurement values in each cycle, yielding lower measurement noise. The shutter time is automatically adjusted by the sensor controller (IFC2471HS, Micro-Epsilon Optronic, Dresden, Germany) between 0.1 and 20 µs.

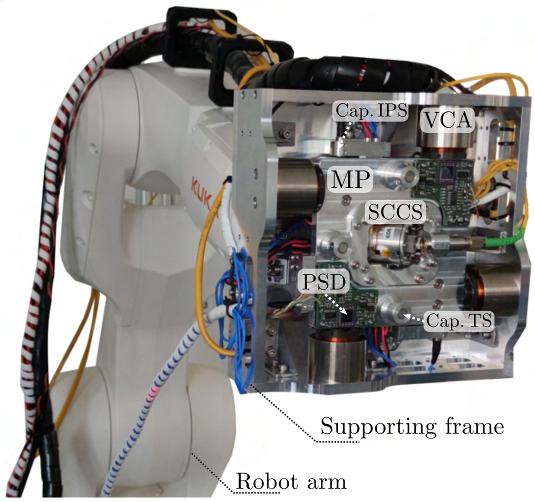

Fig. 2. System prototype with the 3D measurement module mounted to an industrial robot.

3. RELATIVE MOTION CORRECTION

With consideration of the sequentially scanning 3D MT, a synchronized point-by-point correction of the acquired

Post-print version of the article: D. Wertjanz, T. Kern, E. Csencsics, and G. Schitter, "Residual error correction for reducing the uncertainty of a sample-tracking robotic 3D measurement system," *IFAC-PapersOnLine*, vol. 56 (2), 2023, pp. 4418-4423, 2023. DOI: 10.1016/j.ifacol.2023.10.1829

3D point cloud by the measured (residual) relative motion between SCCS and sample is targeted. In a first step, the impact of translational and rotational relative motion on the 3D measurement result is discussed. Based on these findings, a tailored method for post-correcting the residual tracking error for the high-precision robotic measurement system is derived.

3.1 Impact of relative motion

To elaborate on the effect of relative motion on the 3D measurement result, translational and rotational motion of both ,the MP and the sample surface, are considered. In Fig. 3a, a translational in-plane motion Δx relative to a static sample surface is indicated. Consequently, the MS is laterally shifted by $\Delta x_{MS} = \Delta x$. For a translational out-of-plane motion Δz, a similar effect can be observed, which is illustrated in Fig. 3b. The dominant motion-induced measurement error is caused by the axial shift $\Delta z_{MS} \approx \Delta z$. Considering a maximum residual sample-tracking error in DoF z of about $\Delta z = 300\,\mathrm{nm}$ [Wertjanz et al. (2022)] and a full-frame scanning amplitude of about 25 mrad, the additional lateral measurement error is about $300\,\mathrm{nm} \cdot \tan(25\,\mathrm{mrad}) = 7.5\,\mathrm{nm}$, which is about three orders of magnitude smaller than the SCCS' lateral resolution and therefore neglected.

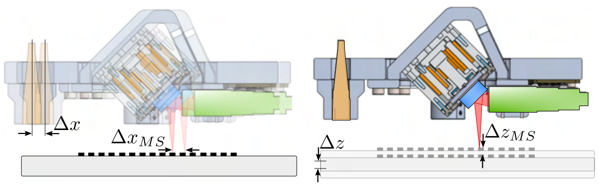

(a) Translational MP motion. (b) Translational sample motion.

Fig. 3. Relative translational motion between MP and sample. a) shows a translational MP in-plane motion Δx, resulting in a lateral shift Δx_{MS} of the MS. A translational out-of-plane sample motion Δz, as indicated in b), yields an axial shift Δz_{MS} of the MS.

In case of relative rotational out-of-plane motion between the MP and the sample, as illustrated in Fig. 4, a uniqueness problem is encountered. In Fig. 4a, the rotational MP motion $\Delta\phi_y$ causes a dominant lateral measurement error of Δx_{MS}. However, a rotational sample motion $\Delta\phi_y$ in the opposite direction (see Fig. 4b) corresponds to the same relative motion measured by the TS system, causing mainly an axial shift Δz_{MS} in the 3D measurement result. Due to this non-uniqueness, rotational relative motion in the out-of-plane DoFs can consequently not be considered in the targeted residual tracking error correction. In contrast, a relative motion between the MP and the sample in the rotational in-plane DoF ϕ_z would cause a uniquely lateral shift of the MS. With consideration of the limited SCCS' lateral scan area of $350 \times 250\,\mu\mathrm{m}^2$ and a typical residual tracking error of 10 µrad, the resulting lateral measurement error is neglectably small and therefore omitted.

3.2 System modelling

In a next step, the method for post-correcting the measured relative motion between the SCCS and the sample

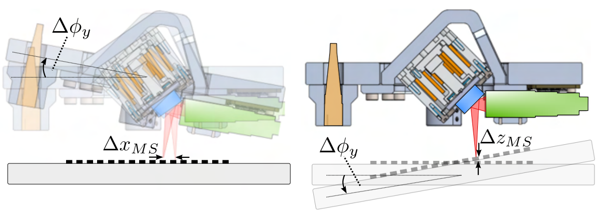

(a) Rotational MP motion. (b) Rotational sample motion.

Fig. 4. Rotational relative motion between MP and sample. The measured relative motion $\Delta\phi_y$ in a) and b) by the TS system is the same, with differently induced effects Δx_{MS} and Δz_{MS} on the position of the MS.

from the point-wise acquired 3D measurement is derived. Based on the measured angular deflection of the FSM's tip- (ϕ) and tilt-axis (θ) together with the distance d measured by the CCS, a measurement point in the 3D point cloud is obtained by applying the calibration-based image reconstruction procedure $\mathbf{F}_{\mathrm{SCCS}}(d, \phi, \theta)$ [Wertjanz et al. (2021)].

Considering the effects of relative motion on the 3D measurement discussed in Section 3.1, an acquired 3D measurement point can be written as

$$\mathbf{P} = \mathbf{F}_{\mathrm{SCCS}}(d, \phi, \theta) + \boldsymbol{\Delta\zeta_t} \tag{1}$$

with $\boldsymbol{\Delta\zeta_t} = [\Delta x, \Delta y, \Delta z]^T$ the unwanted translational motion of the MS due to relative motion. In case of disabled sample-tracking, i.e. the MP stabilized with respect to the robot arm, the translational motion is given by

$$\boldsymbol{\Delta\zeta_t} = \boldsymbol{\zeta_t} - \boldsymbol{\zeta_{t,0}}, \tag{2}$$

with $\boldsymbol{\zeta_t}$ the actual relative position between MP and sample, and $\boldsymbol{\zeta_{t,0}}$ the one at the measurement starting point.

Subtraction of the measured relative translational motion $\boldsymbol{\Delta\tilde{\zeta}_t}$ from (1) yields

$$\mathbf{P_{corr}} = \mathbf{P} - \boldsymbol{\Delta\tilde{\zeta}_t} = \mathbf{F}_{\mathrm{SCCS}}(d, \phi, \theta) + \epsilon_{\boldsymbol{\Delta\zeta_t}}, \tag{3}$$

which is the desired relation to correct the 3D measurement for disabled sample-tracking, with $\epsilon_{\boldsymbol{\Delta\zeta_t}} = \boldsymbol{\Delta\zeta_t} - \boldsymbol{\Delta\tilde{\zeta}_t}$ being the relative translational motion measurement error.

With the sample-tracking control being enabled and $\boldsymbol{\zeta_{t,ref}}$ the relative translational reference position, the residual sample-tracking error

$$\mathbf{e_t} = \boldsymbol{\zeta_t} - \boldsymbol{\zeta_{t,ref}} = [e_x, e_y, e_z]^T \tag{4}$$

is affecting the 3D measurement result. Hence, an acquired 3D measurement point in case of active sample-tracking yields to

$$\mathbf{P_{tr}} = \mathbf{F}_{\mathrm{SCCS}}(d, \phi, \theta) + \mathbf{e_t}. \tag{5}$$

As the residual tracking error is not compensated by the MP but known by measurement of $\mathbf{\tilde{e}_t}$, it can be post-corrected by subtraction from (5), which yields

$$\mathbf{P_{tr,corr}} = \mathbf{P} - \mathbf{\tilde{e}_t} = \mathbf{F}_{\mathrm{SCCS}}(d, \phi, \theta) + \epsilon_{\mathbf{e_t}}, \tag{6}$$

with $\epsilon_{\mathbf{e_t}} = \mathbf{e_t} - \mathbf{\tilde{e}_t}$ being the residual 3D measurement error caused by the translational relative motion for enabled sample-tracking. Consequently, this method does not require any additional hardware.

Post-print version of the article: D. Wertjanz, T. Kern, E. Csencsics, and G. Schitter, "Residual error correction for reducing the uncertainty of a sample-tracking robotic 3D measurement system," *IFAC-PapersOnLine*, vol. 56 (2), 2023, pp. 4418-4423, 2023. DOI: 10.1016/j.ifacol.2023.10.1829

4. EXPERIMENTAL PERFORMANCE EVALUATION

A step height calibration standard (Nanuler Calibration Standard, Applied NanoStructures Inc., Mountain view, CA, USA) with a structural height of 5.81 µm is used as sample surface to investigate the performance of the proposed motion correction method. In Fig. 5a, a microscope image of the selected 3D measurement area is shown. Several surface defects around the selected structural step can be seen. Note, that the rhomboidal shape of the SCCS's lateral measurement area originates from manufacturing and alignment tolerances [Wertjanz et al. (2021)].

The sample is placed on the sample holder [Wertjanz et al. (2022)] and the robotic 3D measurement system is aligned to it, such that the TS system is in range. Lissajous scanning frequencies $f_\phi = 59\,\text{Hz}$ and $f_\theta = 47\,\text{Hz}$ with maximum scan amplitude are applied to the tip- and tilt-axis of the FSM to acquire full-frame images ($350 \times 250\,\mu\text{m}^2$) with the maximum imaging rate of 1 fps. Considering the SCCS' lateral resolution of 2.5 µm as the width of one pixel, the minimum pixel dwell time during the Lissajous scanning at 1 fps is $T_{PD,min} = \frac{2.5\,\mu\text{m}}{300\,\mu\text{m}2\pi 59\,\text{Hz}} \approx 20\,\mu\text{s}$, which is greater than the exposure time of the CCS (see Section 2).

In Fig. 5b, a reference measurement under lab conditions is shown, serving as benchmark for the performance evaluation. As indicated, the surface defects are clearly visible in the 3D image. Within the dashed white rectangle, a mean sample height error of $|e_{top,mean}| = 0.07\,\mu\text{m}$ with an uncertainty of $e_{top,std} = 0.21\,\mu\text{m}$ is achieved. By analyzing the measured sample height along the structure edge (dashed white), an uncertainty of $e_{edge,std} = 0.76\,\mu\text{m}$ is obtained. In Tab. 1, these performance indicators are summarized for an imaging rate of 1 fps and a reduced rate of 0.2 fps, equalling a factor five higher minimum pixel dwell time of 100 µs.

A motor is placed close to the sample box and used as relative motion generator, inducing a mounting structure-dependent resonant vibration according to a workshop environment [Gordon (1999)]. The time signals of the induced relative motion with a frequency of 47 Hz are shown in Fig. 6. As an example, for disabled sample-tracking (red), the resulting translational peak-peak motion between the SCCS and the sample in y is about 125 µm, equalling an RMS motion of 44.5 µm. The corresponding 3D measurements for an imaging rate of 1 fps and 0.2 fps are shown in Figure 5c and 5d. Motion blur corrupts both measurements, with the sample structure being not visible.

4.1 Motion correction for disabled sample-tracking

The performance of the proposed motion correction method is evaluated for disabled sample tracking. Using (3), the measured relative motion is used to correct the 3D measurements shown in Fig. 5c and 5d. The results related to an imaging rate of 1 fps are shown in Fig. 7a. As can be seen, blurry artifacts corrupt the measurement of the structural step, with the surface defects on top of the scan area being not detected. Analyzing the performance indicators, a measurement error in height and an uncertainty on the single micro-meter scale are obtained (see Tab. 1).

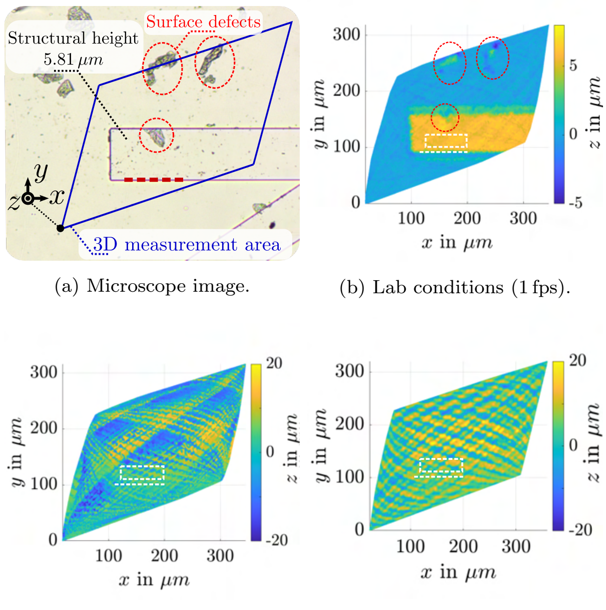

(a) Microscope image. (b) Lab conditions (1 fps).

(c) Tr. OFF; Corr. OFF (1 fps). (d) Tr. OFF; Corr. OFF (0.2 fps).

Fig. 5. Measurement sample. a) shows the microscope image of a structural step with several surface defects within the 3D measurement area. In b), a reference measurement under lab conditions with an imaging rate of 1 fps is shown. In c) and d), the induced relative motion corrupts the measurement results at 1 fps and 0.2 fps.

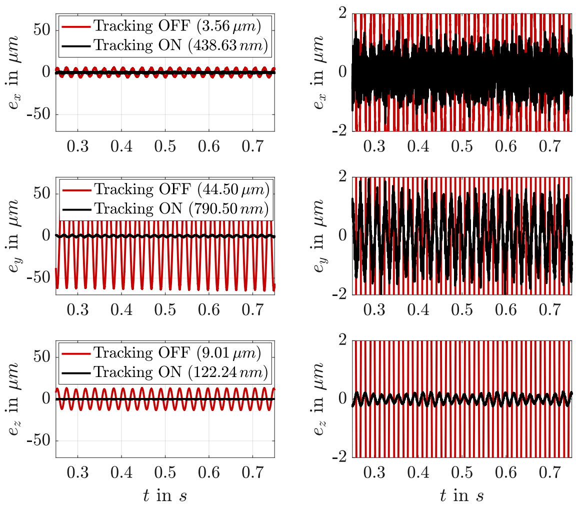

(a) Induced relative motion. (b) Zoomed plot of a).

Fig. 6. Induced relative motion in the translational DoFs. In a), the resonant relative motion for disabled sample-tracking is shown in red. Black indicates the residual tracking error for enabled sample tracking. b) shows a zoomed plot of a). In DoF y, the relative motion of 44.5 µm rms is reduced to 790.50 nm rms.

Post-print version of the article: D. Wertjanz, T. Kern, E. Csencsics, and G. Schitter, "Residual error correction for reducing the uncertainty of a sample-tracking robotic 3D measurement system," *IFAC-PapersOnLine*, vol. 56 (2), 2023, pp. 4418-4423, 2023. DOI: 10.1016/j.ifacol.2023.10.1829

S

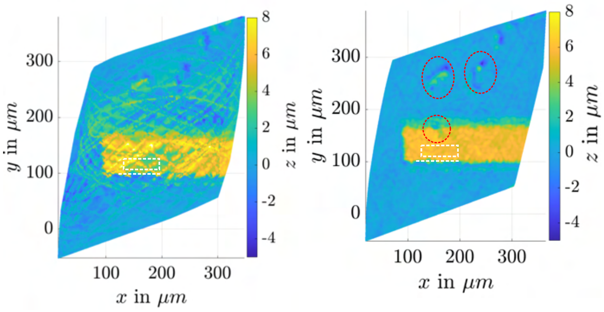

(a) Tr. OFF; Corr. ON (1 fps). (b) Tr. OFF, Corr. ON (0.2 fps).

Fig. 7. 3D measurement results with disabled sample-tracking and applied relative motion correction. In a), blurry artifacts corrupt the measurement at an imaging rate of 1 fps, with the surface defects being not visible. For a reduced scan rate of 0.2 fps in b), the surface defects are detected.

By repeating the experiment for a reduced scan rate of 0.2 fps, the structural step and the surface defects become clearly visible in Fig. 7b. Residual motion blur is especially visible along the horizontal edges of the structural step due to the large relative motion in DoF y (see Fig. 6a). Calculating the standard deviation of the measured sample height along the dashed white cross-section in Fig. 7b, a remaining uncertainty of 1.21 µm is obtained. The performance indicator analysis reveals a height measurement error of 0.21 µm with an uncertainty of 0.33 µm, as summarized in Tab. 1. It is notable, that the SCCS' lateral measurement range is enlarged by about ±62.5 µm in DoF y, which is in good accordance with the measured peak-peak motion of 125 µm.

4.2 Motion correction for enabled sample-tracking

Next, the achieved 3D measurement performance is evaluated for active-sample tracking with and without the proposed residual tracking error correction from (5). The time signal of the residual sample-tracking error for the induced resonant relative motion is indicated in Fig. 6 (black). As can be seen, the 44.5 µm rms motion is reduced to 790.5 nm rms. This equals a relative motion attenuation of 35 dB and is in good accordance with the sensitivity of the tracking control identified in [Wertjanz et al. (2022)].

In Fig. 8a, the state-of-the-art measurement result for a scanning rate of 1 fps is shown. The structural step as well as the surface defects are clearly visible, with an achieved height measurement error and uncertainty of 0.25 µm and 0.35 µm, respectively. Considering the results for the pure motion correction approach in Fig 7a, the 3D imaging performance is increased by a factor of 5.

Finally, the proposed post-correction method of (5) for the measured residual sample-tracking error shown in Fig. 6b (black) is applied to the 3D measurement result in Fig. 8a. The results related to this experiment are shown in Fig. 8b. The residual tracking error correction approach reduces the measurement error and uncertainty of the structural height to 0.19 µm and 0.25 µm, also indicated by the stronger orange color on the structural

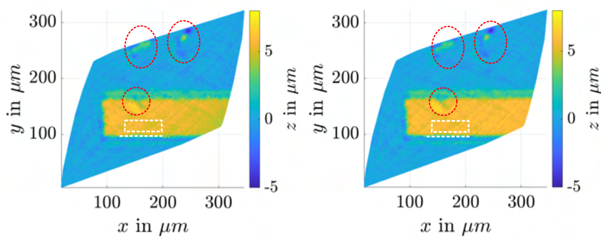

(a) Tr. ON; Corr. OFF (1 fps). (b) Tr. ON; Corr ON (1 fps).

Fig. 8. 3D measurement result for a scan rate of 1 fps with enabled sample-tracking. In a), the result without correcting the residual tracking error is shown. After applying the residual motion correction in b) less uncertainty in the structural height is indicated in stronger orange on the top of the structural step.

top. In addition, the cross-section analysis along the edge (dashed white line) reveals an uncertainty reduction from 0.92 µm to 0.65 µm. For the sake of completeness, the 3D measurement performance results are also shown for a reduced scan rate of 0.2 fps in Tab. 1, indicating a similar performance improvement.

In summary, the residual sample-tracking error correction method for the robotic 3D measurement system reduces the axial measurement error and uncertainty by 20% to 0.19 µm and 0.25 µm for operation at maximum imaging rate in a vibration-prone workshop environment.

5. CONCLUSION

In this paper, a method to correct disturbing relative motion between the high-precision robot-based 3D measurement system and the sample under test is proposed, targeted for the application in a vibration-prone industrial production line. Although disturbing relative motion between the SCCS and the sample can be reduced by means of active sample-tracking, a residual tracking error remains, which limits the achievable 3D measurement performance. The proposed method does not require any additional hardware and enables a point-by-point post-correction of the sequentially acquired 3D point cloud by the measured residual tracking error. For operation at the maximum frame rate of 1 fps, experimental results demonstrate an axial measurement error and uncertainty reduction of 20% to 0.19 µm and 0.25 µm, respectively, in comparison to the state-of-the-art system. In addition, the presented method enables sub-micrometer axial imaging precision of the robotic 3D measurement system for disabled sample-tracking and a reduced scan rate of 0.2 fps, solely by post-correction of the measured relative motion. The results presented in this paper therefore reveal potential system design approaches for future robot-based high-precision inline measurement systems.

REFERENCES

Csencsics, E., Thier, M., Ito, S., and Schitter, G. (2022). Supplemental peak filters for advanced disturbance rejection on a high precision endeffector for robot-based

Table 1. 3D measurement performance comparison.

Frame rate	Performance indicator	Lab environment	Motion corr.	Sample-tr.	Sample-tr. + corr.
1 fps	$\lvert e_{top,mean} \rvert$	0.07 µm	1.42 µm	0.25 µm	0.19 µm
	$e_{top,std}$	0.21 µm	1.57 µm	0.35 µm	0.26 µm
	$e_{edge,std}$	0.76 µm	2.72 µm	0.92 µm	0.65 µm
0.2 fps	$\lvert e_{top,mean} \rvert$	0.03 µm	0.21 µm	0.14 µm	0.08 µm
	$e_{top,std}$	0.18 µm	0.33 µm	0.26 µm	0.21 µm
	$e_{edge,std}$	0.32 µm	1.21 µm	0.70 µm	0.44 µm

inline metrology. *IEEE/ASME Transactions on Mechatronics*, 27(4), 2258–2266.

de Sousa, G.B., Olabi, A., Palos, J., and Gibaru, O. (2017). 3d metrology using a collaborative robot with a laser triangulation sensor. *Procedia Manufacturing*, 11, 132–140.

Fergus, R., Singh, B., Hertzmann, A., Roweis, S.T., and Freeman, W.T. (2006). Removing camera shake from a single photograph. *ACM Transactions on Graphics*, 25(3), 787–794.

Gao, W., Haitjema, H., Fang, F., Leach, R., Cheung, C., Savio, E., and Linares, J. (2019). On-machine and in-process surface metrology for precision manufacturing. *CIRP Annals*, 68(2), 843 – 866.

Gordon, C.G. (1999). *Generic Vibration Criteria for Vibration-Sensitive Equipment*. Colin Gordon & Associates.

Grasso, M. and Colosimo, B. (2017). Process defects and in situ monitoring methods in metal powder bed fusion: a review. *Measurement Science and Technology*, 28, 044005.

Imkamp, D., Schmitt, R., and Berthold, J. (2012). Blick in die Zukunft der Fertigungsmesstechnik - Die VDI/VDE-GMA Roadmap Fertigungsmesstechnik 2020. *Technisches Messen*, 10(79).

Naverschnigg, C., Csencsics, E., and Schitter, G. (2022). Flexible robot-based in-line measurement system for high-precision optical surface inspection. *IEEE Transactions on Instrumentation and Measurement*, 71, 1–9.

Rejc, J., Cinkelj, J., and Munih, M. (2009). Dimensional measurements of a gray-iron object using a robot and a laser displacement sensor. *Robotics and Computer-Integrated Manufacturing*, 25(2), 155–167.

Saathof, R., Thier, M., Hainisch, R., and Schitter, G. (2017). Integrated system and control design of a one dof nano-metrology platform. *Mechatronics*, 47, 88 – 96.

Savio, E., Chiffre, L.D., and Schmitt, R. (2007). Metrology of freeform shaped parts. *CIRP Annals*, 56(2), 810 – 835.

Schitter, G. and Stemmer, A. (2002). Eliminating mechanical perturbations in scanning probe microscopy. *Nanotechnology*, 13(5), 663.

Schlarp, J., Csencsics, E., and Schitter, G. (2020). Design and evaluation of an integrated scanning laser triangulation sensor. *Mechatronics*, 72, 102453.

Schneider, U., Drust, M., Ansaloni, M., Lehmann, C., Pellicciari, M., Leali, F., Gunnink, J., and Verl, A. (2014). Improving robotic machining accuracy through experimental error investigation and modular compensation. *The International Journal of Advanced Manufacturing Technology*, 85, 1–13.

Schwenke, H., Neuschaefer-Rube, U., Pfeifer, T., and Kunzmann, H. (2002). Optical methods for dimensional metrology in production engineering. *CIRP Annals*, 51(2), 685–699.

Wertjanz, D., Kern, T., Csencsics, E., Stadler, G., and Schitter, G. (2021). Compact scanning confocal chromatic sensor enabling precision 3-d measurements. *Appl. Opt.*, 60(25), 7511–7517.

Wertjanz, D., Kern, T., Pechhacker, A., Csencsics, E., and Schitter, G. (2022). Robotic precision 3d measurements in vibration-prone environments enabled by active six dof sample-tracking. In *2022 IEEE/ASME International Conference on Advanced Intelligent Mechatronics (AIM)*, 1441–1446.

Yao, T.F., Duenner, A., and Cullinan, M. (2016). In-line dimensional metrology in nanomanufacturing systems enabled by a passive semiconductor wafer alignment mechanism. *Journal of Micro- and Nano-Manufacturing*, 5(1).

Yogeswaran, A. and Payeur, P. (2012). 3d surface analysis for automated detection of deformations on automotive body panels. In *New Advances in Vehicular Technology and Automotive Engineering*. IntechOpen.

Post-print version of the article: D. Wertjanz, T. Kern, E. Csencsics, and G. Schitter, "Residual error correction for reducing the uncertainty of a sample-tracking robotic 3D measurement system," *IFAC-PapersOnLine*, vol. 56 (2), 2023, pp. 4418-4423, 2023. DOI: 10.1016/j.ifacol.2023.10.1829